- Boron removal by electrocoagulation: removal mechanism, adsorption models and
- 2 factors influencing removal

- 3 Ming Chen^{a,b}, Orion Dollar^a, Karen Shafer-Peltier^b, Stephen Randtke^a, Saad Waseem^c, Edward Peltier^{a,*}
- 4

 ^a Department of Civil, Environmental and Architectural Engineering, University of Kansas, Lawrence, KS,

 5

 66045, USA
- 6

 b Tertiary Oil Recovery Program, University of Kansas, Lawrence, KS, 66045, USA
- 7 ° Department of Chemical and Biomedical Engineering, West Virginia University, Morgantown, WV, 26506, USA
- 9 *Corresponding author: Edward Peltier epeltier@ku.edu
 - **Abstract:** Boron (B), normally present in ground water and sea water, is a vital micronutrient for plants, but is also toxic in excessive amounts. Under typical conditions, aqueous boron is present as boric acid (H_3BO_3), which is uncharged, making B particularly challenging to remove by mechanisms commonly applicable to removal of trace constituents. Adsorption of B onto aluminum hydroxide solids ($AI(OH)_3(s)$) generated using aluminum-based electrocoagulation (EC) is a promising strategy for B removal. Infrared spectroscopy analysis indicated complexation of $B(OH)_3$ with aluminum hydroxide solids via surface hydroxyl groups, while X-ray and infrared spectroscopy results indicated that the structure of the $AI(OH)_3(s)$ was influenced both by EC operating conditions and by water quality. A linear adsorption model predicted B removal well when initial concentrations were lower than 50 mg/L, but fit the experimental data poorly at higher initial B concentrations. The Langmuir adsorption model provided a good fit for a broader range of initial B concentrations (5 1000 mg/L). Factors affecting B adsorption during the EC process, including current intensity, Al dissolution rate, boron concentration, pH, and total

dissolved solid (TDS), were investigated. Increasing current intensity initially led to a higher Al dissolution rate, and therefore higher B adsorption, but there was a limit, as further increases in current intensity caused rapid formation of Al(OH) $_3$ (s) having a large particle size and a low capacity to complex B. Boron removal decreased as its concentration increased. The best removal of B occurred at pH 8, corresponding to a slightly positive zeta potential for aluminum hydroxide and a small but significant fraction of negatively charged B species. Higher TDS concentrations facilitated the use of higher current intensities, i.e., the limit on the effective Al dissolution rate increased with increasing TDS. Two real water samples (river water and oilfield produced water) spiked with B were treated using EC, resulting in up to 50% B removal from river water ($C_0 = 10 \text{ mg/L}$, current = 0.2 A) in 2 hours, and 80% B removal from produced water ($C_0 = 50 \text{ mg/L}$, current = 1.0 A) in 2 hours.

Keywords: Boron removal; electrocoagulation; adsorption model; aluminum hydroxide; surface complex.

1. Introduction

Boron (B) is a naturally occurring element, with freshwater concentrations typically less than 1 mg/L in most regions of the world (WHO, 2003; Hasenmueller and Criss, 2013). Seawater infiltration, boron-rich soils and anthropogenic sources can all result in much higher aqueous boron concentrations, in some cases > 100 mg/L (WHO, 2003; Hasenmueller and Criss, 2013; Chen *et al.*, 2017). Wastewater resulting from oil and gas production (produced waters) is often particularly high in boron content (Sari and Chellam, 2015; Blondes *et al.*, 2017; Chorghe *et al.*, 2017). While boron is an essential plant nutrient at low concentrations (up to 0.3 mg/L), it is toxic to some commercial crops at concentrations that are only marginally greater, from 0.5 - 2 mg/L (Hilal *et al.*, 2011; Yıldırım and Kasım, 2018). Additionally, the World Health Organization

has determined a safe level of boron in drinking water to be 2.4 mg/L (WHO, 2011), although some countries have established stricter standards down to 1.0 mg/L or less (Güler *et al.*, 2015; Guan *et al.*, 2016).

Boron removal is complicated by the properties of aqueous boron species. Boron is present in water as a mixture of boric acid (H_3BO_3 or $B(OH)_3$) and borate ($H_2BO_3^-$ or $B(OH)_4^-$), with the relative amounts of each species depending on pH, as described by the dissociation reaction and equilibrium constant at 25 °C shown in **eq 1** (Dolati *et al.*, 2017). (A predominance area diagram for boric acid is shown in **Figure 15**.)

54
$$B(OH)_3 + H_2O \stackrel{K_a}{\Leftrightarrow} B(OH)_4^- + H^+, \quad pK_a = 9.2$$
 (1)

At near-neutral pH values in dilute solutions (e.g., pH 6 to 8), aqueous B exists mainly as neutrally charged boric acid, which is poorly removed by membrane processes such as reverse osmosis (Xu and Jiang, 2008; Dolati *et al.*, 2017). Increasing the pH above 9 increases boron removal, but adds additional expense and process complexity (Jacob, 2007; Tu *et al.*, 2010). Chemical precipitation using calcium carbonate, hydroxyapatite, and aluminum and iron coagulation have all been studied for boron removal, but again, these processes are more effective when borate, rather than boric acid, is the predominant aqueous phase (Kitano *et al.*, 1978; Sasaki *et al.*, 2016; Chorghe *et al.*, 2017; Dolati *et al.*, 2017). Chorghe *et al.* (2017) found that very high doses of aluminum or iron could remove up to 80% of boron from produced water, but suggested that the amount of chemical required made this approach impractical. While boron-selective ion-exchange resins have been developed, regeneration of these resins requires high chemical dosages, resulting in correspondingly higher material and operational costs (Hilal *et al.*, 2011; Dolati *et al.*, 2017).

Electrocoagulation (EC) is an electrochemical water treatment method that utilizes a sacrificial anode, typically made of aluminum or iron, to generate coagulants in-situ. For EC using aluminum anodes (Al-EC), aluminum ions generated at the anode react with hydroxide ions generated at the cathode, forming a variety of dissolved aluminum hydrolysis products (complexes) and aluminum hydroxide solids, Al(OH)₃(s) (Sari and Chellam, 2015; Chorghe et al., 2017). The distribution of aluminum species formed depends on pH; operating conditions, including current intensity and operating time; and the chemical characteristics of the solution (Ghosh et al., 2008). Electrocoagulation has already seen extensive study for its efficacy in removing a variety of contaminants including total suspended solids (TSS), turbidity, organic matter (as measured by chemical oxygen demand, COD), phosphate and arsenic (Emamjomeh and Sivakumar, 2009; Zhao et al., 2014; Tian et al., 2016). EC also has several reported operational advantages over chemical coagulation, including compact size, simple operation, low capital costs and less waste sludge (Zhang et al., 2016; Shamaei et al., 2018). Several recent studies have examined electrocoagulation for boron removal, with positive results (Ezechi et al., 2014; Isa et al., 2014; Dolati et al., 2017). Sari and Chellam (2015) showed that boron removal from produced waters using EC is achieved primarily through sorption to amorphous Al(OH)₃ precipitates, rather than co-precipitation. Electrocoagulation produces hydroxide ions at the cathode that can react with boric acid to form borate ions, which facilitates increased boron sorption compared to chemical coagulation processes using aluminum or iron sulfate (Dolati et al., 2017).

68

69

70

71

72

73

74

75

76

77

78

79

80

81

82

83

84

85

86

87

88

89

90

91

Electrocoagulation may be particularly suited to boron removal from high-salinity waste streams, including oil produced water. While high background salt concentrations typically hinder other treatment processes, high conductivity decreases the energy requirements for EC operations compared to freshwater conditions. Research to date on B removal by aluminum EC

has given little attention to the removal mechanisms involved, to the adsorptive capacity of Al solids generated under a range of conditions that might alter their characteristics (e.g., structure, morphology and settling rate), and to quantitative models for B adsorption. In particular, the characteristics of Al(OH)₃ solids formed during EC depends both on operating conditions and water composition (e.g., salt concentration) (Wellner *et al.*, 2018) which may have a marked influence on boron adsorption.

The current study uses a two-electrode EC cell to examine the impact of operating parameters and water quality on boron removal through electrochemical generation of dissolved aluminum species. Aluminum hydroxide solids generated during EC were analyzed using X-ray, infrared spectroscopy and dynamic light scattering (DLS) to reveal the relationship between the morphology and structure of EC generated Al(OH)₃(s) and B removal. Quantitative models for B removal were developed based on boron adsorption isotherms and mass balance equations to predict B removal using EC. The specific objectives were: (1) to examine the mechanism(s) of B removal; (2) to develop quantitative models describing B removal by aluminum EC; (3) to optimize B removal by determining the effects of significant operating parameters (especially time and current intensity) and water quality (initial B concentration, pH and TDS); and (4) to experimentally investigate B removal from real waters (e.g., a river water and an oilfield produced water) using aluminum EC.

2. Materials and Methods

2.1 Materials

All reagents were of analytical grade, and were used as received without further purification. Boric acid (99.8%), purchased from Fisher Scientific (Fair Lawn, NJ, US), was used as the boron source. Ultrapure water (18.2 M Ω /cm, Milli-Q Direct 8 system) was used in all

experiments. NaCl was used to adjust the TDS concentration of experimental water samples, while the pH of experimental solutions was adjusted using sodium hydroxide (0.5 M) or nitric acid (2%). The electrodes used for generating aluminum and hydroxide ions in situ consisted of a 99+% aluminum rod anode and 99.999% graphite carbon rod cathode, both purchased from Strem Chemicals (Newburyport, MA, US).

The natural water sample used in this study was collected from the Kansas River, and an oilfield produced water sample was collected from an oil well in Douglas County, KS. The chemical compositions of the water samples are provided in **Tables 1S** and **2S** in the **Supporting Information**. The Kansas River water sample was spiked with 10 mg/L boron and the oilfield produced water was spiked with 50 mg/L boron.

2.2 Electrocoagulation setup and sample collection

The scheme and a photo of the EC cell are shown in **Figure 2S** in the **Supporting Information**. The electrocoagulation reactor consisted of a 150 mL Nalgene plastic beaker with two rods immersed in the aqueous solution, and a Metrohm 804 Ti Stand stirrer. The electrode rods were 1.2 cm in diameter, 5 cm long, and were placed 2.5 cm apart in the solution. Before each experiment, Al electrodes were abraded with sand paper to remove scales and cleaned with 2% HNO₃ and then ultrapure water. An Extech DC regulated power supply (0-30 V) was used as the power source and the electric current was monitored and held constant during each experiment by continuously adjusting the cell voltage. During each experiment, the pH of the solution in the beaker was periodically measured with a pH electrode (Metrohm, 6.0262.100) and adjusted to the target value by the titrator (Metrohm 905 Titrando with 800 Dosino). Because the current interfered with the pH measurement, the current was turned off when pH was measured (Wan et al., 2011).

The total concentrations of B and NaCl (as TDS) in the 150-mL experimental solutions were 50 mg/L and 2000 mg/L, respectively, except when explicitly described otherwise. Every 15 or 30 min during each experiment, 2-4 mL of solution were collected from the beaker, and a 1 mL aliquot was diluted by 2% HNO3 to 10 mL and analyzed to determine the total concentrations of B and Al in the solution. The rest of the sample was filtered using a 0.45 µm Nylon filter (Fisherbrand), and 1 mL of the filtrate was acidified and diluted with 2% HNO3 to 10 mL, then used to determine the dissolved concentrations of selected elements. The concentrations of B and Al were determined using an inductively coupled plasma-optical emission spectrometer (ICP-OES, PerkinElmer, Optima 2000 DV). Triplicate ICP analyses were performed for each sample, and measurements accepted if all results were within 10% of the averaged value. The difference between the total and dissolved concentrations represented B removed from solution and the amount of Al precipitate formed. Aluminum hydroxide solids concentrations are reported herein in mg/L as Al.

To compare the EC process with conventional alum coagulation, boron removal experiments were conducted using solid aluminum sulfate (16-hydrate) as a coagulant. Solid aluminum sulfate was added directly to the solution at varying dosages. After alum addition, the pH was adjusted back up to the desired value, the beaker sealed and stirred for one and a half hours, and the suspension was left to settle for 24 hours. A sample of the supernatant was then collected, acidified, and analyzed for boron using ICP as described above.

2.3 Precipitate analysis

After selected experiments, aluminum solid samples were collected after standing for 24 h (without stirring) in the beaker to measure their size distribution. The mean particle size of the Al solids was determined by dynamic light scattering (DLS) using a NanoBrook Omni particle

sizer (Brookhaven Instruments Corp.). Three consecutive 1-min measurements were obtained while detecting light scattering at a 90° angle. The mean effective diameter was determined by the method of cumulants (Cordova *et al.*, 2008).

Samples of Al coagulant solids were collected, dried, and prepared for FTIR and XRD analysis after selected EC experiments. Al coagulant solids were collected by filtering each treated sample through a 10 kDa ultrafiltration membrane (shown in **Figure 3S** in the **supporting information**). The resulting filter cakes were frozen at less than -20°C. The frozen samples were then freeze-dried in a Labconco Freezone 4.5 and ground to obtain powder with <5% moisture. Complexation between B and Al coagulants was characterized using attenuated total reflectance Fourier-transform infrared spectroscopy (ATR-FTIR, Agilent Technologies Cary 630). The structure of Al coagulant samples was examined using X-ray diffraction (XRD, Bruker D2 PHASER) with a Co K α radiation source (λ = 1.79026 Å) operated at 30 kV and 10 mA, and the 2 θ scanning angle ranged from 25° to 100° with a speed of 11°/min.

2.4 Predictive model of boron removal

The B removal fraction during electrocoagulation, η , can be calculated by eq 2,

176
$$\eta = 1 - \frac{[B]_{aq}}{[B]_{total}} \tag{2}$$

where $[B]_{total}$ and $[B]_{aq}$ refer to the total and aqueous concentrations, respectively, of B in solution in mg/L.

Boron removal was modeled as an adsorptive process with B adsorbing on Al solids (eq 3).

Al solids production was a function of time and current intensity (eq 4), while the total concentration of B in the beaker remained constant (eq 5).

182
$$[B]_{Al} = f([B]_{aq})$$
 (3)

$$183 m = f(t, I) (4)$$

184
$$[B]_{total} = \frac{m}{V}[B]_{Al} + [B]_{aq}$$
 (5)

In these equations, $[B]_{AI}$ refers to the concentration of B on Al coagulant solids, mg/g; m is the mass of Al dissolved from anode and precipitated as Al coagulant solids, g; t and I represent EC operating time and current, with units of s and amperes (A), respectively; and V is the volume of the EC reactor, in L. Once the adsorption model (eq 3) and mass of Al solids (eq 4) are determined, B removal can be predicted under a range of different conditions (Chen and Jafvert, 2017, 2018a).

3 Results and Discussion

3.1 Aluminum dissolution as a function of current intensity

Aluminum dissolution rates as a function of EC reaction time at varying current intensities are shown in **Figure 1** for a solution at pH 8 with 2000 mg/L NaCl. The current intensities ranged from 0.1 to 1.4 A and were kept constant by continuously adjusting the cell voltage during each experiment (0-2 h). The relationship between the current (I) and the amount (I) of aluminum dissolved in the EC reactor over time (I) can be theoretically predicted using Faraday's law (Moussa *et al.*, 2017) (**eq 6**), which was used to plot the lines shown in **Figure 1a**.

$$199 m = \frac{IMt}{zF} (6)$$

where I refers to current flow, A, and M is the atomic weight of AI, 27 g/mol; t represents operating time, s; z is the number of electrons transferred in the reaction at the electrode (z=3)

electrons per mole of AI, based on the reaction $Al(s) \rightarrow Al^{3+}(aq) + 3e^-$ occurring at the anode); and F is Faraday's constant, 96,486 C/mol.

The faradaic efficiency (FE) of Al generated during EC, or the percentage of actual to theoretical Al production, can be calculated based on **eq 7** (Lv *et al.*, 2014), to describe the charge transfer efficiency in a system facilitating an electrochemical reaction.

$$FE = \frac{zNF}{lt} \times 100\% \tag{7}$$

where *N* is the amount of the generated products in the EC process, in mole Al; and the remaining parameters are the same as in **eq 6**. **Figure 1b** shows the faradaic efficiency of the EC cell at different current intensities and reaction times.

From **Figure 1a**, experimental Al dissolution rates were slightly elevated compared to theoretical predictions using Faraday's law (**eq 6**) for currents ranging from 0.10 A to 0.50 A. Previous studies (Yilmaz *et al.*, 2007; Sari and Chellam, 2015) have also observed a similar trend. The observed super-faradaic dissolution may be caused by the presence of chloride ions, which can adsorb onto the oxide passivation film on the Al anode surface, and react with Al species in the oxide film, reducing the thickness of the oxide film as a result of chemical dissolution (Mouedhen *et al.*, 2008; Sari and Chellam, 2015). Additionally, the chloride ions also cause pitting corrosion which produces small pits or holes on the Al electrode surface, leading to elevated metallic aluminum loss (Mameri *et al.*, 1998; Jiménez-Come *et al.*, 2012; Wellner *et al.*, 2018). From **Figure 1b**, currents from 0.10 to 0.50 A all produced FE values above 100% during the 2 h EC process, consistent with observed super-faradaic dissolution. Based on a regression of the experimental data (0.10-0.50 A), the mean ratio of the actual dissolution of the Al anode to

Faraday's law model lines (i.e., the mean FE values) was 1.16. (This is similar to the average value of all single FE values, 1.17).

223

224

225

226

227

228

229

230

231

232

233

234

235

236

237

238

239

241

The faradaic efficiency at the two highest currents was much lower than at 0.5 A or lower. The FE at 0.70 A started to decrease at 60 min, where FE was $^{\sim}$ 1, then decreased markedly to around 0.6 at 120 min. At 1.40 A, FE decreased dramatically after only 30 min (to 0.6) and remained below 0.8 at 60 min. The low faradaic efficiencies were likely caused by passivation of the Al anode. The high dissolution rates of Al at these currents caused rapid formation of a stable oxidized film that covers and passivates the Al anode, inhibiting the further dissolution of Al to the solution, which increases resistance and reduces efficiency (Badawy et al., 1999). The "pitting corrosion" effect of the high chloride ion concentration is slower than this passivating process. The passivation behavior of electrodes is a serious concern for the longevity of the EC process (Kabdaşlı et al., 2012), particularly given the increasingly early passivation effects as current increased.

To better predict the amount of Al released under the conditions of this study, including the effects of super-faradaic dissolution, the average FE value (1.16) was applied as a modification factor to current intensities ≤ 0.50 A, and the value of m in the Al mass balance model (eq 4) was determined using a modified Faraday's law (eq 8),

$$240 m = FE \frac{IMt}{zF} (8)$$

Based on the experimental data, FE = 1.16 was used for all experiments in this study when the 242 current intensity was 0.50 A or less.

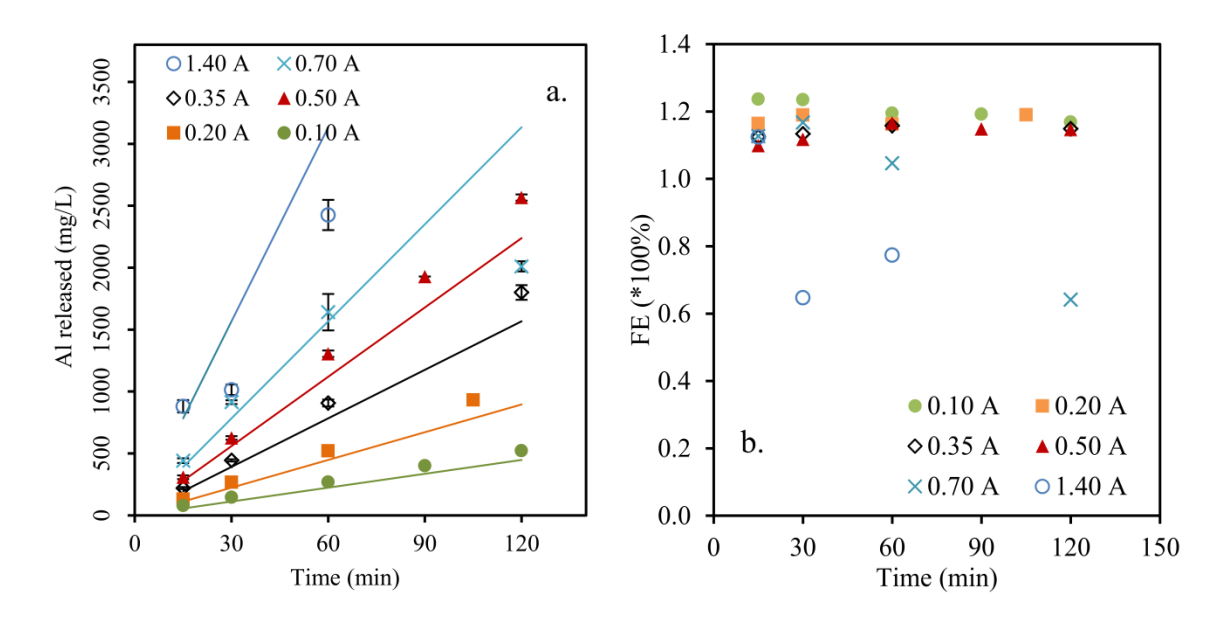


Figure 1. Aluminum dissolution during EC: (a) Al concentration as a function of time and current intensity (Lines are predictions based on Faraday's law.); (b) Faradaic efficiency of Al generation.

3.2 Boron complexation with aluminum hydroxide solids

Figure 2 shows the ATR-FTIR results for dried Al(OH)₃(s) precipitated using the electrocoagulation process at pH 8 both with and without boron present in solution. The boron solution initially contained 50 mg/L B, of which approximately 65% was removed to the solid phase. Two new peaks associated with B removal appeared at around 1433 cm⁻¹ and 1280 cm⁻¹ for Al(OH)₃(s). These peaks are also distinct from those for boric acid in a saturated B(OH)₃ solution, which were observed at 1403 cm⁻¹ and 1144 cm⁻¹, in agreement with previously reported spectra (Su and Suarez, 1995). These results indicate complexation of boron on the Al(OH)₃(s) surface, leading to formation of a strong Al-O-B bond. The peak close to 1430 cm⁻¹ appears due to B-O asymmetric stretching, and the peak near 1280 cm⁻¹ arises because of inplane bending of trigonal boron (Su and Suarez, 1995). Chorghe *et al.* (2017) also reported broad peaks at similar wavelengths (1426 cm⁻¹ and 1312 cm⁻¹) in an alum coagulated NaCl solution containing 130 mg/L B, which were interpreted as depicting boron trigonally coordinated with

Al(OH)₃(s). Lefèvre (2004) reported peaks at 1420 and 1280 cm⁻¹ for Al(OH)₃(s) paste with adsorbed B at pH 7, indicating strengthening of O-B and B-OH bonds in the surface complex \equiv Al-O-B(OH)₂. Sari and Chellam (2015) reported that the adsorption of B on Al(OH)₃(s) was based on outer-sphere and inner-sphere complexation of B(OH)₃ with Al(OH)₃, confirmed by the B-O bond shifting toward lower binding energies in XPS.

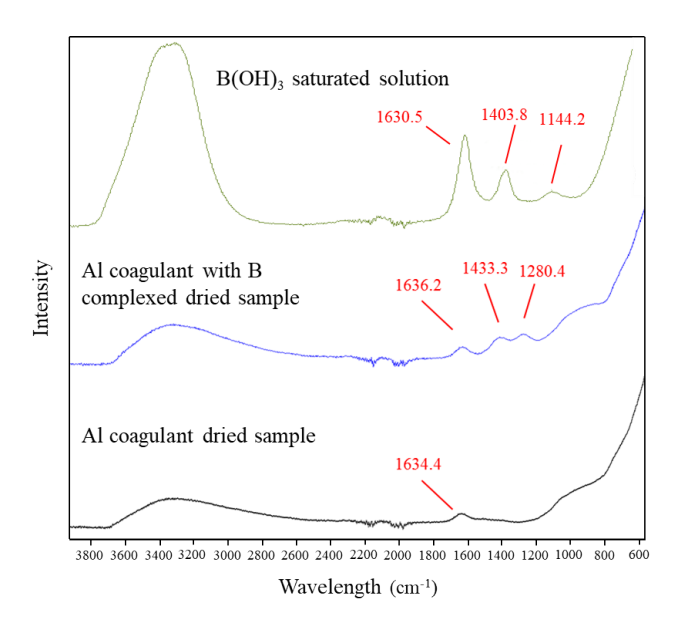


Figure 2. FTIR of boron complexation with aluminum hydroxide solids

3.3 Boron removal using Al-EC at varying current intensities

Figure 3 shows boron removal by EC, using an Al anode at pH 8, as a function of time and the applied current. As shown in Figure 3a, increasing B removal was observed with increasing time and with increasing current for currents ranging from 0.10 A to 0.50 A. As the total applied electric charge is the product of current and time, increasing operation time or current both result in a greater total applied charges. From 0.10-0.50 A current intensity, boron removal increased with increasing applied charge (Figure 4S in the Supporting Information). The highest

removal of B, 70%, was observed in 2 h at 0.50 A. Dolati *et al.* (2017) also reported 70% B removal, from a solution with an initial B concentration of 100 mg/L, using aluminum EC at pH 8.

For a current of 0.70 A, B removal was higher than that obtained using 0.50 A during the first 30 min, but then increased only 10% from 30 min to 2 h, resulting in much lower overall removal. At 1.40 A, boron removal was below that at 0.35 A at 30 minutes. These results indicate that using too high a current adversely affects B removal by Al-EC. One of the possible reasons for this is that Al ion generation is inhibited (as shown in **Figure 1**) by the formation of a passive layer on the Al anode at high currents. Other possible reasons involve changes in the morphology and structure of the Al(OH)₃(s) formed in the reaction, which will be discussed in the following section.

Figure 3b shows the relationship between B removal and Al dose (i.e., total Al generated by Al-EC or added in the form of aluminum sulfate) for both Al-EC (using currents of 0.10 to 0.50 A) and coagulation using aluminum sulfate. The model line is based on the model described in Section 3.4. Boron removal increased as more Al ions were generated, with 70% removal of B achieved by EC at an Al dose of around 2.5 g/L. Yilmaz et al. (2007) observed even higher B removal, up to 94% when generating at Al dose of 7.45 g/L during the Al-EC process. It can be seen that B removal by Al-EC was much higher than that achieved using coagulation with aluminum sulfate when comparing the two processes based on total Al added, e.g., ~60% removal for Al-EC at 1500 mg/L Al, versus only ~40% removal by coagulation with aluminum sulfate. There are several possible explanations for the higher B removal during EC. The continuous generation of Al(OH)₃(s) due to Al dissolution over time in the EC system may allow more B to incorporate into the Al solid structure as it forms and aggregates, while the rapidly formed Al(OH)₃(s) produced by chemical coagulation may result in less surface contact area or

time for B incorporation. Additionally, hydroxide generated at the electrode results in locally high pH values that could induce formation of negatively charged B(OH)₄, which would adsorb better to the Al solids.

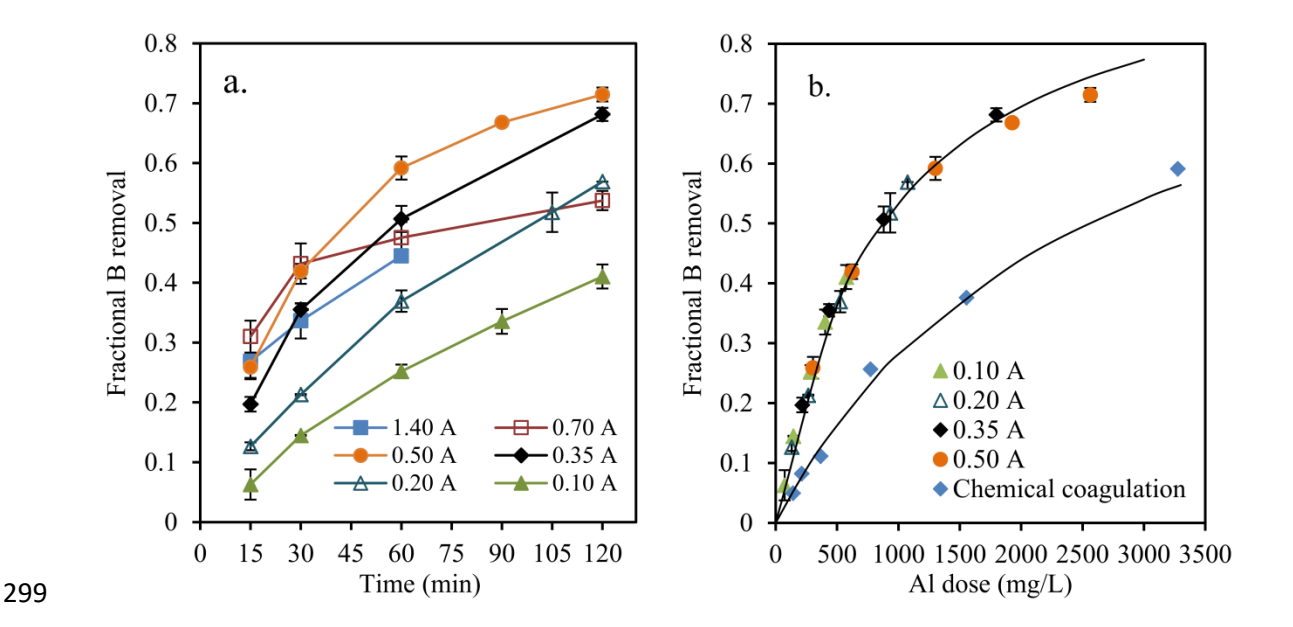


Figure 3. Boron removal at pH 8 at varying current intensities: (a) *versus* operating time; (b) *versus* Al dose for current intensities of 0.10 A to 0.50 A, with the results compared to model results (solid line) and to chemical coagulation with aluminum sulfate. (Initial B concentration =

50 mg/L; NaCl = 2000 mg/L)

To investigate the effect of Al dissolution rate (i.e., current) on B removal, samples were compared based on the B removal observed after the same concentration of Al (~900 mg/L) was generated (with longer operating times being required for samples treated with lower currents).

Figure 4a shows B removal by Al-EC with currents of 0.20, 0.35, 0.70, and 1.40 A, which required operating times of 105, 60, 30, and 15 min, respectively, to generate about 900 mg/L of Al ions.

Currents of 0.20 A and 0.35 A produced similar B removal (~52%), higher B removal than observed using 0.70 A (~43%) and 1.40 A (~27%). Particles generated using the 1.40 A current

settled rapidly (< 30 minutes), while those generated at lower currents required several hours to settle and formed a less compact floc layer (photo, **Figure 4b**). Mean effective size measurements collected after allowing the particles to stand for 24 hours (**Figure 4b**) show that the solids generated with a current of 1.40 A were much larger than those in the other samples, with the largest mean effective size of ~120 μ m. The Al solids generated by currents of 0.20 A and 0.35 A had essentially identical mean particles sizes, while the particles at 0.7 A were larger, but still much smaller than those at 1.40 A.

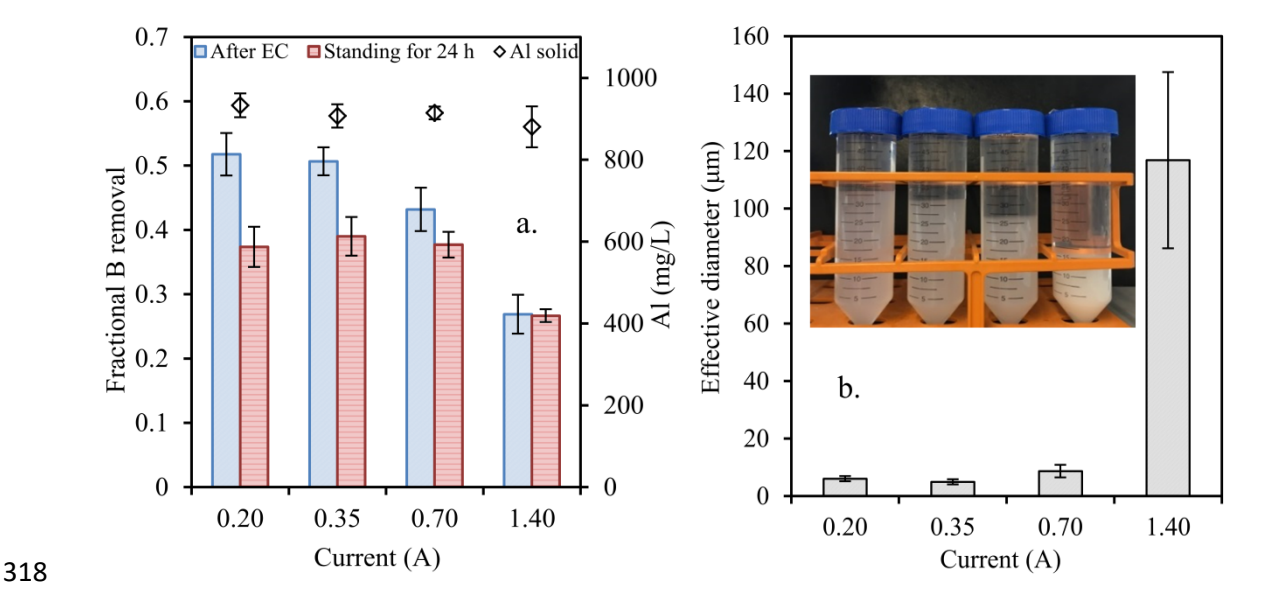


Figure 4. Boron removal *versus* current when generating the same total Al solid concentration (~900 mg/L): (a) B removal initially (in samples filtered immediately after Al-EC treatment) and after 24 hours (samples filtered); (b) Mean effective sizes of the Al(OH)₃(s) particles and a photo showing the relative volumes and appearance of the solids after 24 h of settling.

Figure 4a also shows that boron was released from the Al(OH)₃ solids between initial collection and 24 hours, except for those of larger particle size produced by the 1.40 A current.

B release from these samples ranged from 6 to 15% and can be explained by structural changes

in the Al(OH)₃(s), as shown in **Figure 5**. XRD analysis (**Figure 5a**) shows no obvious peaks for the Al(OH)₃(s) generated using a 0.35 A current and collected immediately after Al-EC, but distinct peaks in the solids generated with 1.40 A. After contact with the solution for 24 h, the 0.35 A solids also show the same peaks as initially observed in the higher current sample. FTIR spectroscopy (**Figure 5b**) of these samples shows a similar pattern. The initial solids generated at 0.35 A have only one peak, at 1634 cm⁻¹, while the 24 h aged sample shows two new peaks at 1063 and 879 cm⁻¹, which are similar to the peaks at 1065 and 880 cm⁻¹ for the initial sample generated by high current (1.40 A). Liu *et al.* (2012) reported similar peaks (1072 and 884 cm⁻¹) for boehmite (γ -AlOOH). The color of Al(OH)₃(s) generated at 0.35 A also changed visibly from gray to white during the 24 h period, as shown in **Figure 3S** in the **Supporting Information**.

The XRD and FTIR results indicate that Al(OH)₃(s) solids generated by Al-EC using a lower current intensity are initially more amorphous and better able to complex with B to form Al-O-B bonds. As the solids gradually crystallize, a portion of the B is released as some of the Al-O-B bonds are slowly transformed to Al-O-Al bonds. Wu *et al.* (2019) also reported observing structural changes in Al(OH)₃(s), evidenced by similar XRD and FTIR analyses, indicating a shift from amorphous to more crystalline structure after 24 h. Based on their study, given enough time (which can be affected by stirring or other processes), Al solid would form boehmite structure. The small-intensity peaks in the XRD pattern for Al solids obtained immediately after production at 1.40 A indicate some crystal structure is already present in these precipitates, with characteristics similar to boehmite, which is consistent with the FTIR results (Liu *et al.*, 2012). Al solids analyzed immediately after reaction at 0.35 A show no evidence of crystal structure in their XRD pattern. However, ageing for 24 hours produces the same peaks as those found in the 1.40 A sample at shorter times. These results, particularly in comparison to Wu et

al.'s results, indicate that Al solids produced from EC form similar phases under both conditions, but that crystallization is much faster at higher currents.

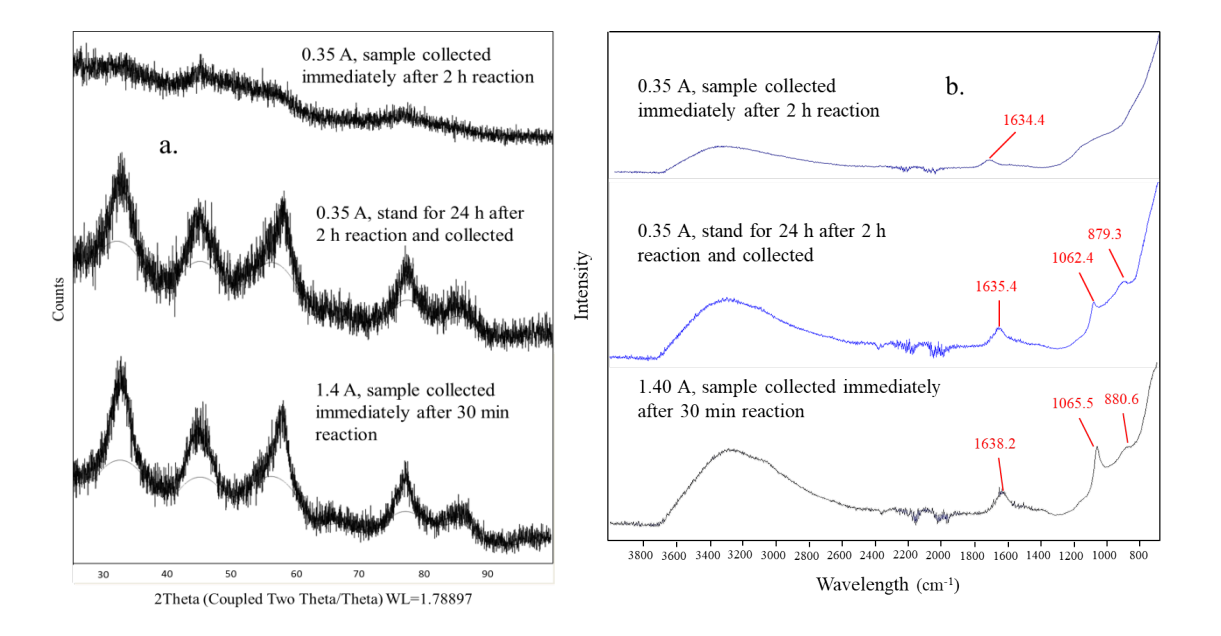


Figure 5. (a) XRD and (b) FTIR analysis of Al(OH)₃(s) samples generated at 0.35 or 1.40 A

3.4 Boron adsorption models

To obtain a better view of boron removal over a wider concentration range, EC experiments were conducted at pH 8 using initial B concentrations ranging from 5 to 1000 mg/L and current of 0.5 A. The results are shown in **Figure 6a**, and the classic Langmuir adsorption isotherm (**eq 9**) (Chen and Jafvert, 2018b) was used to express B concentrations on the Al(OH)₃(s) as a function of the aqueous B concentration.

359
$$[B]_{Al} = \frac{K[B]_{aq}[B]_{max}}{1 + K[B]_{aq}}$$
 (9)

where $[B]_{Al}$ and $[B]_{aq}$ refer to the B concentrations in the solid phase (Al(OH)₃(s)) (mg/g) and aqueous phase (mg/L), respectively; K represents the Langmuir adsorption constant, calculated

based on data shown in **Figure 6a** as 0.0021 L/mg, and $[B]_{max}$ is the calculated maximum B concentration adsorbed on Al coagulant, 538 mg/g.

As can be seen from **Figure 6a**, when the aqueous B concentration is < 100 mg/L the relationship is approximately linear, so a linear model (**eq 10**) can be used to predict B removal at low initial concentrations. Using the data shown in **Figure 3** and the same background aqueous conditions (total B concentration of 50 mg/L at pH 8) and currents ranging from 0.10 A to 0.50 A, a boron adsorption isotherm for Al(OH)₃(s) was simply regressed using a linear adsorption model (**eq 10**),

370
$$[B]_{Al} = a[B]_{ag}$$
 (10)

where a is the linear adsorption constant, and was found from linear regression to be 1.14 L/g for our experimental data (**Figure 6b**, R²=0.96). (Using a similar approach to model B removal by coagulation with aluminum sulfate, as shown in **Figure 3b**, the "a" value was only 0.392, showing the lower affinity of boron for Al(OH)3 produced through chemical coagulation.)

Figure 6c shows B removal using EC with varying initial concentrations at pH 8. B removals were similar for B initial concentrations of 5 mg/L and 50 mg/L, which were higher than for an initial B concentration of 250 mg/L, and the data show a clear trend of decreasing B removal as the initial B concentration increased. Yilmaz et al. (2007) showed that B removal decreased as initial concentration increased from 100 mg/L to 1000 mg/L for both EC and chemical coagulation. On the contrary, Dolati et al. (2017) reported that removal of B declined when the initial B conentration was reduced from 100 mg/L to 10 mg/L. A predictive model (Section 2.4) describing B removal by Al-EC was developed by coupling the linear adsorption model (eq 10) for an initial B concentration of 50 mg/L with mass balances on B (eq 5) and Al (eq 8). As can be seen in Figure 6c, the predictive model was in reasonably good agreement with experimental

values for initial B concentrations of 5 and 50 mg/L, but the model did not predict the observed decrease in boron removal at 250 mg/L.

Figure 6d shows B removal *versus* initial B concentration after 15 and 30 min of Al-EC treatment at 0.50 A, which produced about 320 and 640 mg/L of Al(OH)₃(s), respectively. The results clearly show that B removal decreased with increasing initial B concentration, confirming the earlier results (Figure 6c). Combining a Langmuir adsorption isotherm with the mass balance equation yields predictions in good agreement with experimental data for a broad range of initial B concentrations and for varying Al concentrations, and much better predictions for high initial B concentrations than those when using the linear adsorption model. As boron concentrations increase, the deviation between the two models also increases, as shown in Figure 6d. Indeed, the values predicted using the Langmuir adsorption model were also in good agreement with the experimental data for an initial B concentration of 250 mg/L shown in Figure 6c (model lines shown in Figure 5S). In summary, the Langmuir model can be used to describe B removal by EC from various water environmental conditions over a broad range of initial B concentrations (e.g., freshwater, seawater, wastewater or produced waters), while the linear model is reasonably accurate only for initial B concentrations of 100 mg/L or less.

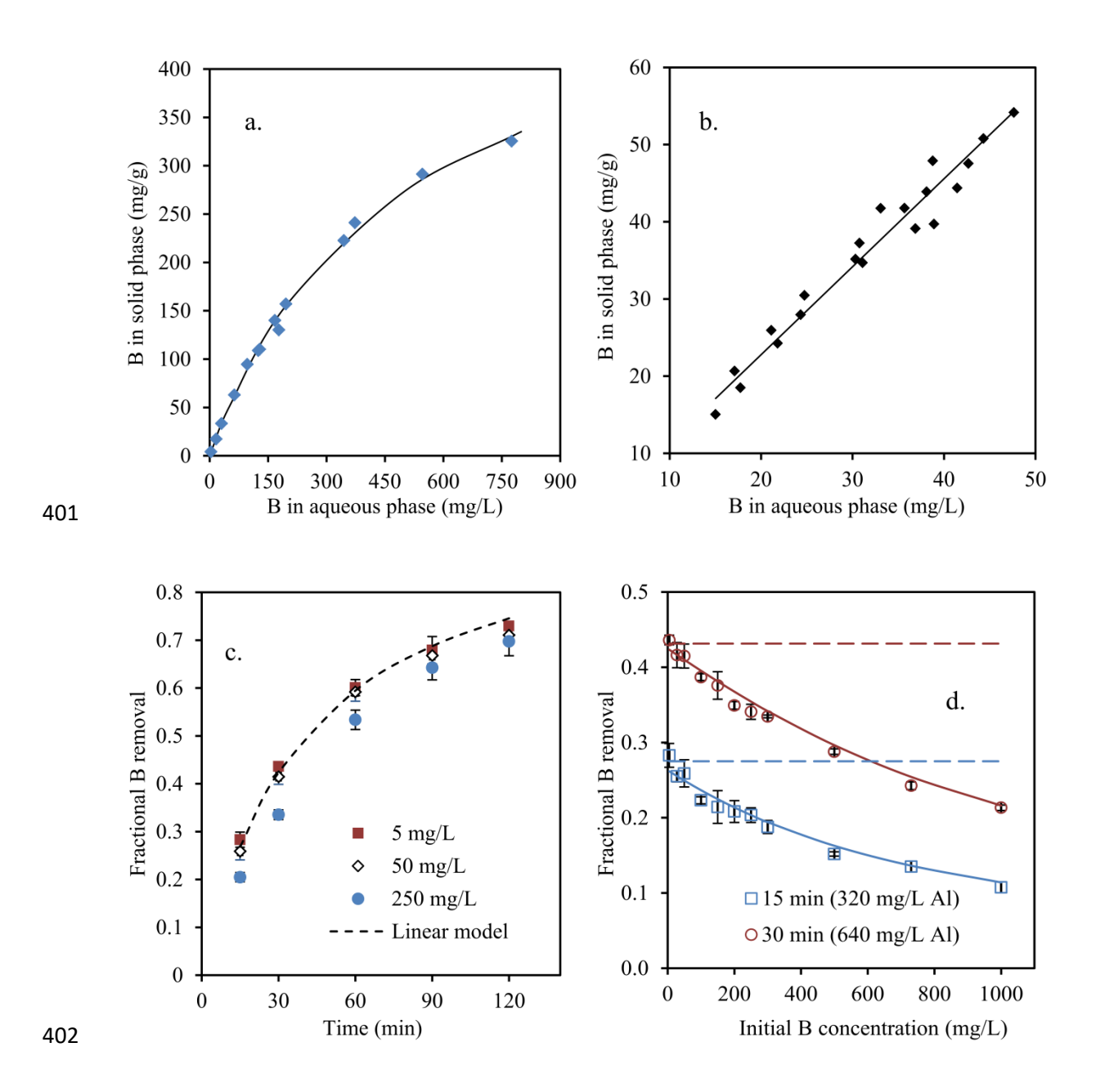


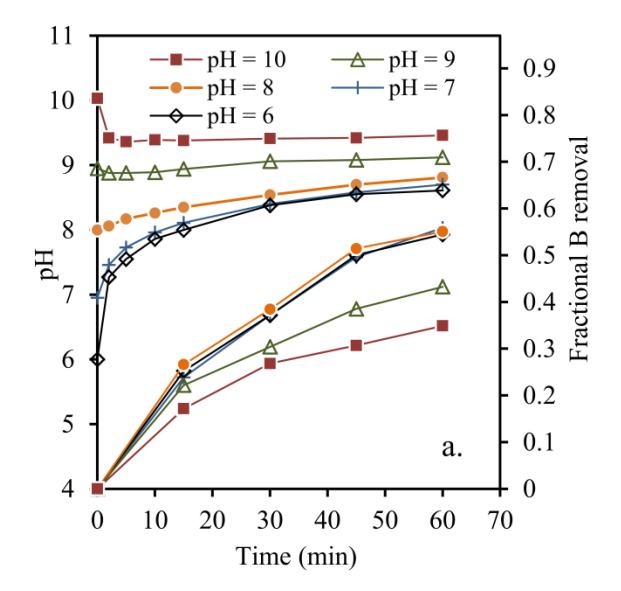
Figure 6. Modeling boron removal by Al-EC: (a) Langmuir adsorption isotherm for initial B concentrations ranging from 5 mg/L to 1000 mg/L; (b) Linear adsorption isotherm for an initial B concentration of 50 mg/L; (c) Boron adsorption with varying initial B concentrations compared to linear model for an initial B concentration of 50 mg/L; (d) Comparison of Langmuir model (solid lines) and linear B removal model (dashed lines) to removal data at 0.5 A for higher initial boron concentrations.

3.5 Effect of pH on boron adsorption

Solution pH has a notable impact on boron removal using Al-EC. **Figure 7a** shows fractional B removal as a function of time for various initial pH values when the pH was not controlled during the EC process (In these experiments, the current was 0.50 A, the initial B and NaCl concentrations were 50 mg/L, and 2000 mg/l, respectively, and initial pH was adjusted by adding HNO₃ or NaOH before EC process.). For starting pH values between 6 and 8, pH increased over time to a final pH of about 8.5 after one hour. For a starting pH of 10, the pH decreased quickly to 9.4 during the first 5 min, then remained constant for the rest of the experiment. For a starting pH of 9, the pH stayed relatively constant throughout the experiment. The final B removals (after 1 h) were similar for starting pH values between 6 and 8, and higher than those obtaining with an initial pH of 9 or 10. The stabilization of pH over time is attributed to the buffering effect of boric acid. Sayiner *et al.* (2008) reported that the pH values of B solutions in iron and aluminum EC systems changed sharply until a maximum value was reached, then remained relatively stationary, in similar fashion to what was observed for the aluminum EC system in this study.

Boron removal at constant pH values ranging from 6 to 10 is shown in **Figure 7b.** Boron removal increased with increasing pH from 6 to 8, and then decreased at higher pH values of 9 and 10. The best removal of B occurred at pH 8 with approximately 40% removal at 30 min, and 60% at 60 min. These results were virtually the same as those of Yilmaz *et al.* (2005), who also reported that a pH of 8 was optimal for B removal by EC with aluminum. EC produced similar amounts of solids at initial pH values of 7, 8 and 9, but slightly less at pH 6 (presumably due to formation of more positively charged soluble Al hydroxo complexes) and much less at pH 10, which is attributable to the formation of substantial amounts of tetrahydroxoaluminate ions,

Al(OH)₄. A pH of 8 was also found to be optimal for boron removal by alum coagulation (**Figure 6S**). The zeta potential of the Al solids produced by Al-EC at varying pH values is shown in **Figure 7c**. Zeta potential decreased with increasing pH, as expected, switching from positive to negative at pH slightly below 9. Based on the dissociation of boric acid ($pK_a = 9.2$, **eq 1**), at pH 9 less than half of the B would be present in the form of negatively charged borate ions. At higher pH values, the concentration of borate ions increases, but so does the negative charge on the Al solids according to Al(OH)₃ stability diagram (Kartikaningsih *et al.*, 2016). At a pH of 8, less than 10% of the B is present as borate ions, but as borate ions are bound to the positively charged Al(OH)₃(s) solids, additional borate ions form and then are removed. Although the zeta potential of Al solids is higher at pH 6 and 7, the fraction of negatively charged B species is negligible, and neutrally charged boric acid is not attracted to the positively charged Al solids.



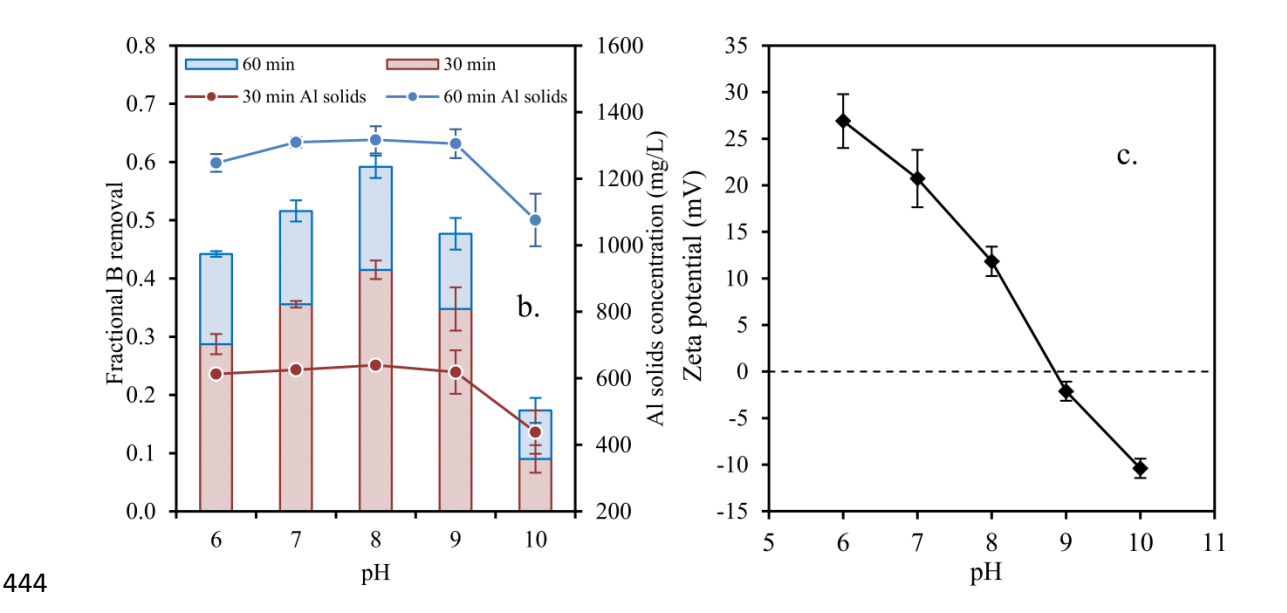
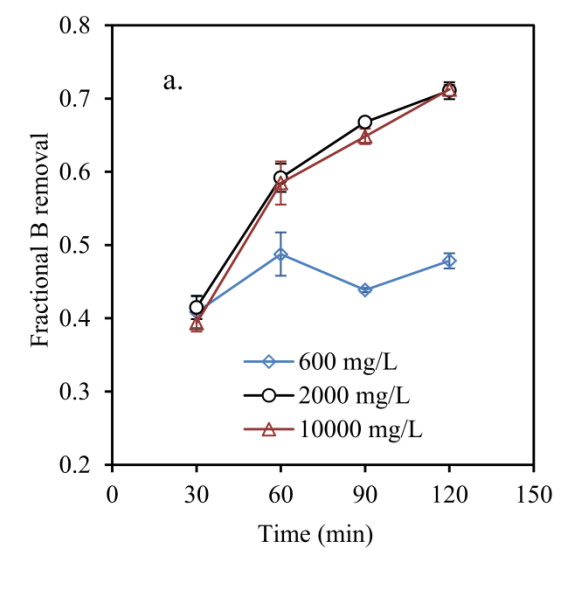


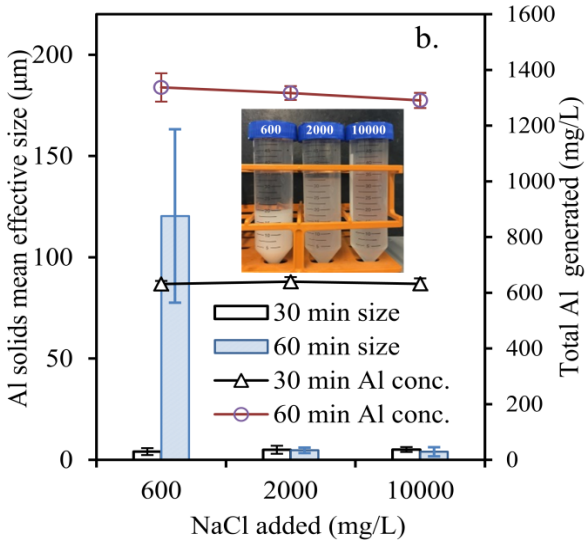
Figure 7. pH effect on boron removal by Al-EC using a current of 0.50 A: (a) Boron removal and pH changes during Al-EC treatment with an initial B concentration of 50 mg/L; (b) Boron removal after 30 and 60 min. for selected constant pH values; (c) Zeta potential of Al solids after 60 min at selected constant pH values.

3.6 Effect of TDS on boron adsorption

Figure 8 shows the effect of varying the NaCl (TDS) concentration on B removal using Al-EC at pH 8. Boron removal using a current of 0.50 A was around 40% for solutions with 600, 2,000, and 10,000 mg/L NaCl (Figure 8a). In high TDS solutions (2,000 and 10,000 mg/L NaCl), B removal increased as time and Al generation increased, with up to 70% removal at 2 h. However, B removal did not increase after 60 min for the 600 mg/L NaCl solution, and decreased at 90 min. Figure 8b shows the mean effective sizes of Al solids at 30 min and 60 min for each solution. At 30 min, when the concentration of Al solids was around 640 mg/L, the effectives size of the Al solids in varying TDS solutions were similar; all were around 5 μm. But at 60 min, the effective size of the Al solids in the 600 mg/L NaCl solution increased dramatically to

120 μm, much larger than those of the solids in the other two solutions, although all of the solutions had similar total Al solids concentrations. As can be seen in the picture in Figure 8b, the sedimentation performance of the Al solids in the 600 mg/L NaCl solution was also better than those of the solids in the other two solutions. Lee and Gagnon (2016) also reported that EC formed larger, more compact flocs in low salt solutions. These results indicate that higher TDS (or ionic strength) leads to Al solids with a more amorphous structure and worse sedimentation performance, but better adsorption of B than the more crystalline solids formed at low TDS. In addition, TDS was increased by adding NaCl. With increased chloride ion concentration the removal of passivating layers on Al anode surface accelerates, allowing the reaction to act in a super-faradaic capacity. Electrode passivation in high chloride solutions is therefore reduced at equivalent operating conditions. For these reasons, higher TDS (NaCl) concentrations facilitate use of higher current intensities, i.e., the limit on the Al generation rate for achieving optimal B removal increases with increasing TDS. Figure 8c confirms this conclusion by demonstrating that a lower current intensity (0.35 A) led to similar B removal in the 600 and 2000 mg/L NaCl solutions in 2 h.





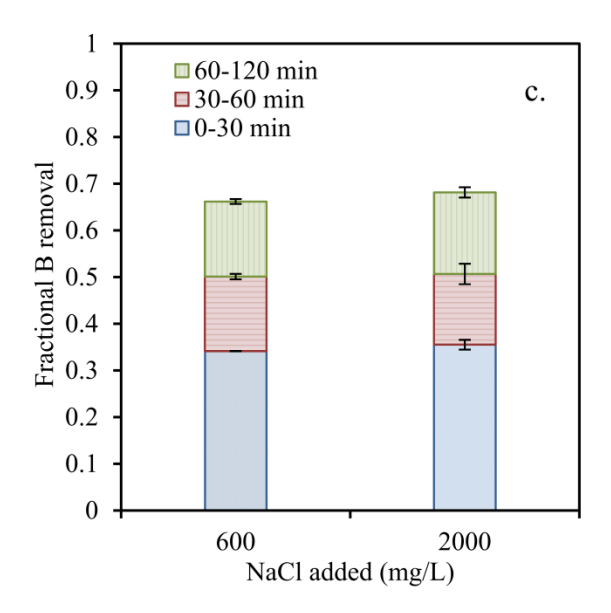


Figure 8. Boron removal by Al-EC from solutions with varying NaCl concentrations: (a) Boron removal *versus* time at 0.50 A; (b) Mean effective size of Al solids and total Al generated after 30 and 60 min at 0.50 A; (c) Boron removal over time at 0.35 A with 600 and 2,000 mg/L as NaCl added.

3.7 Boron removal from natural and produced waters by Al-EC

Figure 9 shows boron removal at pH 8 from a Kansas River water sample and an oilfield produced water sample, both collected in Douglas County, KS. For the Kansas River water sample spiked with 10 mg/L B (Figure 9a), B removal increased with increasing time. Up to 50% B removal was achieved in 2 h using 0.20 A, and the removals predicted (using the Langmuir adsorption model) were close to the experimental values. Using 0.35 A, B removal increased during the first hour, and exceeded the removal achieved using 0.20 A, but decreased after that. The model predicted removals were much greater than the experimental values and the difference increased after 1 h. A likely reason for these results is that given the low TDS of the

Kansas River water, the 0.35 A current began generating more crystalline solids after 1 h, which reduced the solids' capacity to adsorb B.

Figure 9b shows B removal from an oilfield produced water sample spiked with 50 mg/L B. Because the TDS of the water sample was much higher than that of Kansas River water (31,000 mg/L; see Table 2S), higher currents were applied. B removal increased over time at both 0.5 A and 1.0 A, and up to 80% B was removed in 2 h with a 1.0 A current. The gaps between model predictions and experimental data were large during the first hour, but became smaller at 90 min and 120 min. Possible reasons why B removal was less than predicted include: 1) the high conductivity caused by high TDS (31,000 mg/L) may adversely affect contaminant removal during the EC process because the corresponding high ionic strength clearly affects the kinetics and equilibria of reactions between charged species (Lin and Peng, 1994; Can *et al.*, 2003); and 2) removal of divalent cations (or hardness, e.g., Ca²⁺, Mg²⁺, Ba²⁺, and Sr²⁺), which occurred primarily during the first hour (as shown in Figure 7S), may have altered the composition and characteristics of the Al solids and affected their ability to adsorb B (Brahmi *et al.*, 2016; Hakizimana *et al.*, 2016).

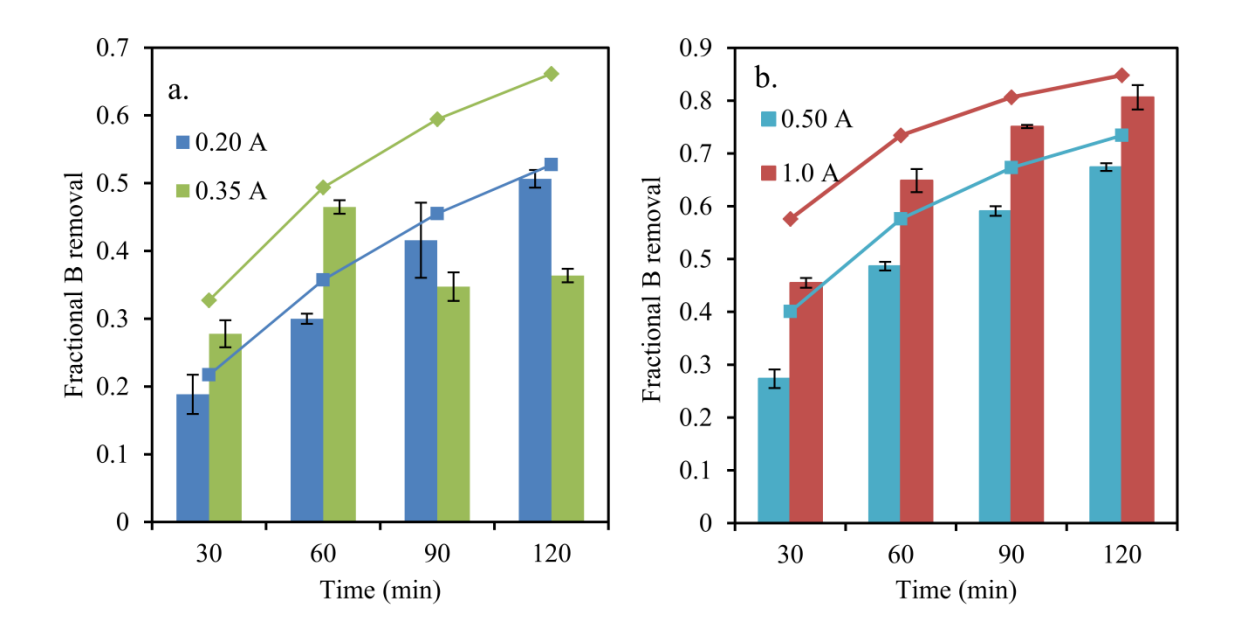


Figure 9. Boron removal by Al-EC from real water samples spiked with B: (a) Kansas River water spiked with 10 mg/L B; (b) Oilfield produced water from Douglas County, KS, spiked with 50 mg/L B. (Lines show Langmuir model predicted values.)

Conclusions

505

506

507

508

509

510

511

512

513

514

515

516

517

518

519

520

521

522

523

524

525

526

527

Under typical water quality conditions, aqueous boron (B) is present primarily as boric acid (H₃BO₃), which is neutrally charged, making B particularly challenging to remove. This research investigated B removal using electrocoagulation (EC), with aluminum and carbon electrodes electrolytically dissolving aluminum ions into the water to act as a coagulant. FTIR analysis showed the formation of surface complexes of B with Al solids (Al(OH)₃(s)), providing a pathway for B removal from solution. B removal increased with Al dissolution (and Al solids formation), and electrocoagulation was found to achieve better B removal than coagulation with aluminum sulfate when the same amount of Al was added. More amorphous Al solids with a higher B adsorption capacity are formed using low currents, while more crystalline solids with a lower adsorptive capacity for B, but better sedimentation properties, are formed using higher currents. The optimal pH for AI-EC was found to be 8. A linear adsorption model was found to be suitable for predicting B removal for initial B concentrations up to 50 mg/L. At higher initial B concentrations of B, the linear model over-predicted B removal, but the Langmuir adsorption model predicted B removal by Al-EC reasonably well for initial B concentrations ranging from 5 to 1,000 mg/L, provided that the current was low enough to avoid formation of less amorphous Al solids. The limiting current depends strongly on the TDS concentration; samples having a higher TDS concentration, such as produced water, can tolerate a higher current without forming solids having a lower adsorptive capacity for B. Two real water samples (a river water and an oilfield produced water), both spiked with B, were treated using the AI-EC process. Up to

50% of the B was removed from the river water (spiked with 10 mg/L of B) in 2 hours with a 0.2 A current; and 80% of the B was removed from produced water (spiked with 50 mg/L B) in 2 hours with a 1.0 A current.

Acknowledgements

This study was financially supported by the National Science Foundation EPSCoR Track-2 Research Infrastructure Improvement Program: Track-2 Focused EPSCoR Collaboration award (OIA-1632892). We also would like to thank Mohammad Sirwan Alimoradi, Kyle Stephens, and Stacy Tinner for their help with sample collection and XRD analysis.

536

537

528

529

530

531

532

533

534

535

References

538 Badawy, W., Al-Kharafi, F. and El-Azab, A., 1999. Electrochemical behaviour and corrosion inhibition of Al, Al-6061 and Al–Cu in neutral aqueous solutions. Corros. Sci. 41(4), 709-727. 539 540 Blondes, M.S.G., Engle, M., Kharaka, Y., Reidy, M., Saraswathula, V., Thordsen, J., Rowan, E. and 541 E., M., 2017. U.S. Geological Survey National Produced Waters Geochemcial Database v 2.3, US 542 Geological Survey, Reston, VA. 543 Brahmi, K., Bouguerra, W., Belhsan, H., Elaloui, E., Loungou, M., Tlili, Z. and Hamrouni, B., 2016. 544 Use of electrocoagulation with aluminum electrodes to reduce hardness in Tunisian phosphate 545 mining process water. Mine Water Environ. 35(3), 310-317. 546 Can, O.T., Bayramoglu, M. and Kobya, M., 2003. Decolorization of Reactive Dye Solutions by 547 Electrocoagulation Using Aluminum Electrodes. Ind. Eng. Chem. Res. 42(14), 3391-3396. 548 Chen, M. and Jafvert, C.T., 2017. Anion exchange on cationic surfactant micelles, and a 549 speciation model for estimating anion removal on micelles during ultrafiltration of water. 550 Langmuir 33(26), 6540-6549.

- 551 Chen, M. and Jafvert, C.T., 2018a. Anion recovery from water by cross-linked cationic surfactant
- 552 nanoparticles across dialysis membranes. Environ. Sci. Nano 5(6), 1350-1360.
- 553 Chen, M. and Jafvert, C.T., 2018b. Application of cross-linked stearic acid nanoparticles with
- dialysis membranes for methylene blue recovery. Sep. Purf. Technol. 204, 21-29.
- 555 Chen, Z., Taylor, A.A., Astor, S.R., Xin, J. and Terry, N., 2017. Removal of boron from wastewater:
- 556 Evaluation of seven poplar clones for B accumulation and tolerance. Chemosphere 167, 146-154.
- 557 Chorghe, D., Sari, M.A. and Chellam, S., 2017. Boron removal from hydraulic fracturing
- wastewater by aluminum and iron coagulation: Mechanisms and limitations. Water Res. 126,
- 559 481-487.
- 560 Cordova, M., Cheng, M., Trejo, J., Johnson, S.J., Willhite, G.P., Liang, J.-T. and Berkland, C., 2008.
- Delayed HPAM gelation via transient sequestration of chromium in polyelectrolyte complex
- nanoparticles. Macromolecules 41(12), 4398-4404.
- Dolati, M., Aghapour, A.A., Khorsandi, H. and Karimzade, S., 2017. Boron removal from aqueous
- solutions by electrocoagulation at low concentrations. J. Environ. Chem. Eng. 5(5), 5150-5156.
- 565 Emamjomeh, M.M. and Sivakumar, M., 2009. Review of pollutants removed by
- electrocoagulation and electrocoagulation/flotation processes. J. Environ. Manage. 90(5), 1663-
- 567 1679.
- 568 Ezechi, E.H., Isa, M.H., Kutty, S.R.M. and Yaqub, A., 2014. Boron removal from produced water
- using electrocoagulation. Process Saf. Environ. 92(6), 509-514.
- 570 Ghosh, D., Solanki, H. and Purkait, M., 2008. Removal of Fe (II) from tap water by
- 571 electrocoagulation technique. J. Hazard Mater. 155(1-2), 135-143.
- 572 Guan, Z., Lv, J., Bai, P. and Guo, X., 2016. Boron removal from aqueous solutions by adsorption—
- 573 A review. Desalination 383, 29-37.

- Güler, E., Kaya, C., Kabay, N. and Arda, M., 2015. Boron removal from seawater: state-of-the-art
- 575 review. Desalination 356, 85-93.
- Hakizimana, J.N., Gourich, B., Vial, C., Drogui, P., Oumani, A., Naja, J. and Hilali, L., 2016.
- 577 Assessment of hardness, microorganism and organic matter removal from seawater by
- 578 electrocoagulation as a pretreatment of desalination by reverse osmosis. Desalination 393, 90-
- 579 101.
- Hasenmueller, E.A. and Criss, R.E., 2013. Multiple sources of boron in urban surface waters and
- 581 groundwaters. Sci. Total Environ. 447, 235-247.
- 582 Hilal, N., Kim, G. and Somerfield, C., 2011. Boron removal from saline water: a comprehensive
- 583 review. Desalination 273(1), 23-35.
- Isa, M.H., Ezechi, E.H., Ahmed, Z., Magram, S.F. and Kutty, S.R.M., 2014. Boron removal by
- 585 electrocoagulation and recovery. Water Res. 51, 113-123.
- Jacob, C., 2007. Seawater desalination: Boron removal by ion exchange technology. Desalination
- 587 205(1), 47-52.
- 588 Jiménez-Come, M.J., Muñoz, E., García, R., Matres, V., Martín, M.L., Trujillo, F. and Turias, I.,
- 589 2012. Pitting corrosion behaviour of austenitic stainless steel using artificial intelligence
- 590 techniques. J. Appl. Log. 10(4), 291-297.
- 591 Kabdaşlı, I., Arslan-Alaton, I., Ölmez-Hancı, T. and Tünay, O., 2012. Electrocoagulation
- 592 applications for industrial wastewaters: a critical review. Environ. Technol. Rev. 1(1), 2-45.
- Kartikaningsih, D., Shih, Y.-J. and Huang, Y.-H., 2016. Boron removal from boric acid wastewater
- 594 by electrocoagulation using aluminum as sacrificial anode. Sustain. Environ. Res. 26(4), 150-155.
- 595 Kitano, Y., Okumura, M. and Idogaki, M., 1978. Coprecipitation of borate-boron with calcium
- 596 carbonate. Geochem. J. 12, 183-189.

- 597 Lee, S.Y. and Gagnon, G.A., 2016. Comparing the growth and structure of flocs from
- 598 electrocoagulation and chemical coagulation. J. Water Process Eng. 10, 20-29.
- Lefèvre, G., 2004. In situ Fourier-transform infrared spectroscopy studies of inorganic ions
- adsorption on metal oxides and hydroxides. Adv. Colloid Interface Sci. 107(2-3), 109-123.
- 601 Lin, S.H. and Peng, C.F., 1994. Treatment of textile wastewater by electrochemical method.
- 602 Water Res. 28(2), 277-282.
- 603 Liu, C., Shih, K., Gao, Y., Li, F. and Wei, L., 2012. Dechlorinating transformation of propachlor
- through nucleophilic substitution by dithionite on the surface of alumina. J. Soil. Sediment. 12(5),
- 605 724-733.
- 606 Lv, W., Zhang, R., Gao, P. and Lei, L., 2014. Studies on the faradaic efficiency for electrochemical
- reduction of carbon dioxide to formate on tin electrode. J. Power Sources 253, 276-281.
- 608 Mameri, N., Yeddou, A.R., Lounici, H., Belhocine, D., Grib, H. and Bariou, B., 1998. Defluoridation
- 609 of septentrional Sahara water of North Africa by electrocoagulation process using bipolar
- aluminium electrodes. Water Res. 32(5), 1604-1612.
- 611 Mouedhen, G., Feki, M., Wery, M.D.P. and Ayedi, H., 2008. Behavior of aluminum electrodes in
- electrocoagulation process. J. Hazard. Mater. 150(1), 124-135.
- 613 Moussa, D.T., El-Naas, M.H., Nasser, M. and Al-Marri, M.J., 2017. A comprehensive review of
- 614 electrocoagulation for water treatment: Potentials and challenges. J. Environ. Manage. 186, 24-
- 615 41.
- Sari, M.A. and Chellam, S., 2015. Mechanisms of boron removal from hydraulic fracturing
- 617 wastewater by aluminum electrocoagulation. J. Colloid Interf. Sci. 458, 103-111.
- 618 Sasaki, K., Toshiyuki, K., Ideta, K., Miki, H., Hirajima, T., Miyawaki, J., Murayama, M. and Dabo, I.,
- 619 2016. Removal mechanism of high concentration borate by co-precipitation with hydroxyapatite.
- 620 J. Environ. Chem. Eng. 4(1), 1092-1101.

- 621 Sayiner, G., Kandemirli, F. and Dimoglo, A., 2008. Evaluation of boron removal by
- 622 electrocoagulation using iron and aluminum electrodes. Desalination 230(1-3), 205-212.
- 623 Shamaei, L., Khorshidi, B., Perdicakis, B. and Sadrzadeh, M., 2018. Treatment of oil sands
- 624 produced water using combined electrocoagulation and chemical coagulation techniques. Sci.
- 625 Total Environ. 645, 560-572.
- 626 Su, C. and Suarez, D.L., 1995. Coordination of adsorbed boron: A FTIR spectroscopic study.
- 627 Environ. Sci. Technol. 29(2), 302-311.
- Tian, Y., He, W., Zhu, X., Yang, W., Ren, N. and Logan, B.E., 2016. Improved electrocoagulation
- reactor for rapid removal of phosphate from wastewater. ACS Sustain. Chem. Eng. 5(1), 67-71.
- Tu, K.L., Nghiem, L.D. and Chivas, A.R., 2010. Boron removal by reverse osmosis membranes in
- 631 seawater desalination applications. Sep. Purif. Technol. 75(2), 87-101.
- 632 Wan, W., Pepping, T.J., Banerji, T., Chaudhari, S. and Giammar, D.E., 2011. Effects of water
- chemistry on arsenic removal from drinking water by electrocoagulation. Water Res. 45(1), 384-
- 634 392.
- 635 Wellner, D.B., Couperthwaite, S.J. and Millar, G.J., 2018. Influence of operating parameters
- during electrocoagulation of sodium chloride and sodium bicarbonate solutions using aluminium
- electrodes. J. Water Process Eng. 22, 13-26.
- 638 WHO, 2003. Boron in drinking water, World Health Organization, Geneva, Switzerland.
- 639 WHO, 2011. Guidelines for drinking-water quality, fourth ed, World Health Organization, Geneva,
- 640 Switzerland.
- 641 Wu, M., Yu, W., Qu, J. and Gregory, J., 2019. The variation of flocs activity during floc breakage
- and aging, adsorbing phosphate, humic acid and clay particles. Water Res. 155, 131-141.
- Xu, Y. and Jiang, J.-Q., 2008. Technologies for boron removal. J. Ind. Eng. Chem. 47(1), 16-24.

644 Yıldırım, K. and Kasım, G.Ç., 2018. Phytoremediation potential of poplar and willow species in 645 small scale constructed wetland for boron removal. Chemosphere 194, 722-736. 646 Yilmaz, A.E., Boncukcuoğlu, R. and Kocakerim, M.M., 2007. A quantitative comparison between 647 electrocoagulation and chemical coagulation for boron removal from boron-containing solution. 648 J. Hazard. Mater. 149(2), 475-481. 649 Yilmaz, A.E., Boncukcuoğlu, R., Kocakerim, M.M. and Keskinler, B., 2005. The investigation of 650 parameters affecting boron removal by electrocoagulation method. J. Hazard. Mater. 125(1-3), 651 160-165. 652 Zhang, X., Lin, H. and Hu, B., 2016. Phosphorus removal and recovery from dairy manure by 653 electrocoagulation. RSC Adv. 6(63), 57960-57968. 654 Zhao, S., Huang, G., Cheng, G., Wang, Y. and Fu, H., 2014. Hardness, COD and turbidity removals 655 from produced water by electrocoagulation pretreatment prior to reverse osmosis membranes. 656 Desalination 344, 454-462.